Available online at www.sciencedirect.com

ScienceDirect

Green Energy & Environment 2 (2017) 294–301

www.keaipublishing.com/gee

Research paper

Proton dynamics in phosphotungstic acid impregnated mesoporous silica proton exchange membrane materials

Krystina Lamb [a], Richard A. Mole [b], Dehong Yu [b], Roland de Marco [a,c,d], John R. Bartlett [a], Sarah Windsor [a], San Ping Jiang [d], Jin Zhang [d], Vanessa K. Peterson [b,*]

[a] *Faculty of Science, Health, Education and Engineering, University of the Sunshine Coast, Sippy Downs, Queensland 4556, Australia*
[b] *Australian Centre for Neutron Scattering, Australian Nuclear Science and Technology Organisation, Lucas Heights, New South Wales 2234, Australia*
[c] *School of Chemistry and Molecular Biosciences, The University of Queensland, Brisbane, Queensland 4072, Australia*
[d] *Fuels and Energy Technology Institute, Curtin University, Perth, Western Australia 6109, Australia*

Received 21 April 2017; revised 17 June 2017; accepted 24 June 2017
Available online 8 July 2017

Abstract

Phosphotungstic acid is an excellent proton conductor that can be incorporated into porous supports, and nanocomposite proton exchange membrane materials made from mesoporous silica impregnated with phosphotungstic acid have been suggested for use in fuels cells operating > 100 °C. In this work, quasielastic neutron scattering was used to study proton self-diffusion in mesoporous disordered and *P6mm* symmetry silica impregnated with two concentrations of phosphotungstic acid. Overall, the silica structure had a significantly greater effect on proton conduction and diffusion than phosphotungstic acid concentration, with higher proton conduction occurring for the *P6mm* symmetry silica samples. Quasielastic neutron scattering revealed two populations of protons diffusing through each sample, and that proton conduction is limited by the slower of these populations, which diffuse via a jump-diffusion mechanism. Whilst the fundamental jump-diffusion mechanism by which these slower protons moved was found to be similar for both silica supports and phosphotungstic acid concentrations, the faster diffusion occurring in *P6mm* structured silica arises from a lower residence time of protons moving between sites in the jump-diffusion model, suggesting a lower energy barrier.

Keywords: Fuel cells; Neutron scattering; Proton conduction; Proton exchange membranes; Silica

1. Introduction

The development of proton-exchange membrane fuel cells (PEMFCs) for portable energy production is attractive due to the high power density of liquid and gas fuels, such as methanol, ammonia, and liquid petroleum gas. The present low temperatures of operation of PEMFCs (~80 °C) have a number of issues, such as low tolerance to impurities, low value heat and problems with water management. Increasing the operating temperature of proton exchange membranes (PEMs) to 100–200 °C has many benefits, such as reduced need for humidification, increased in catalytic activity of the electrodes, improved heat recovery, and higher tolerance to impurities in the fuel stream. Much work has been done to develop low cost and high conductivity inorganic materials as alternative PEMs for this purpose [1]. In particular, inorganic framework materials such as mesoporous silica have shown promise, and although the proton conductivity of such materials under fully hydrated conditions is too low for function as PEMs, the incorporation of proton carriers into these structures can significantly enhance proton conductivity, making them viable for this purpose. Phosphotungstic acid (HPW), $[PW_{12}O_{40}]^{3-}$, a member of the Keggin type heteropoly acid

* Corresponding author.
E-mail address: vanessa.peterson@ansto.gov.au (V.K. Peterson).

http://dx.doi.org/10.1016/j.gee.2017.06.007

group, has one of the highest known proton conductivities. HPW has been shown to be a good electrolyte for low temperature PEMs, although its water solubility results in leaching from the electrolyte membrane without anchoring to a substrate such as silica [2].

Following this first work using PEMs constructed from HPW anchored to silica, highly ordered phosphotungstic acid functionalised-mesoporous silica nanocomposite (HPW-MSN) PEMs tolerant to the conditions within direct alcohol fuel cells have been subsequently produced [3–8]. Single cell tests were performed using a 30 wt.% HPW-impregnated *P6mm*-symmetry mesoporous silica membrane of thickness ~0.8 mm with a Pt/C catalyst anode and cathode, which reveals a low permeability of the HPW-MSN and an open circuit voltage of 0.97 V, very close to that of single cells assembled with Nafion® membranes [4–6]. Despite the thick electrolyte, the maximum power density of cells assembled with the HPW-MSN was 24 mW cm^{-2} at 25 °C and 95 mW cm^{-2} at 100 °C, demonstrating the applicability of HPW-MSN as a fuel cell PEM [4–6].

Previous work studying HPW-MSN PEMs revealed their conductivity to be highly dependent on hydration level, HPW concentration, and type of silica support [3–8]. Such effects are difficult to understand, primarily because the exact mechanism of proton conduction in HPW-MSN is largely unknown. Generally, proton diffusion is thought to occur in HPW-MSNs via a jump-diffusion process [9]. Molecular dynamics simulations have shown the shortest jump distance for a proton moving between two HPW Keggin units in HPW-MSN to be ~1.6 Å, with an energy requirement that is lower than for intra-Keggin hopping within the material [9]. This study also demonstrated that proton conduction was correlated strongly to increasing water and HPW concentration, to a limit.

HPW crystallizes with $Pn\bar{3}m$ symmetry in which the distance between two HPW units is 12.6 Å, where each Keggin unit is ~5.5 Å in radius [10]. Theoretical studies using density functional theory (DFT) have showed that proton jumps between charged sites within Keggin units in anhydrous HPW have a high activation energy, 103.3 kJ mol^{-1}, dropping to 11.2 kJ mol^{-1} under hydrated conditions [11], explaining somewhat the hydration-dependent conductivity. Further, combined solid-state nuclear-magnetic resonance (NMR) and DFT calculations showed that protons in anhydrous HPW were located at both bridging and terminal oxygens, and that isolated protons are immobile at room temperature, but hydrated acidic protons were highly mobile [12]. This work revealed that under semi- and fully-hydrated conditions protons associated with the outer HPW oxygen were highly mobile. However, these studies did not take the silica matrix into account.

A study on the proton conductivity of mesoporous silica and porous silica glass showed the attachment/release of protons from hydroxyl groups on the pore surface, noting that conduction in these materials is ~4 orders of magnitude lower than in HPW [13]. NMR studies found that in silica-HPW systems one of the three protons associated with the HPW is donated to the silica surface, inducing a net positive charge on the silica surface which contributes to anchoring the charged molecules [14,15].

Quasielastic neutron scattering (QENS) is an excellent tool to elucidate the mechanism of proton diffusion underpinning conduction as it can directly measure proton dynamics [16]. QENS spectra, $S(\boldsymbol{Q}, \omega)$, are dependent on the magnitude of the scattering vector, $\boldsymbol{Q} = \boldsymbol{k_i} - \boldsymbol{k_f}$, $(4\pi/\lambda)\sin(\theta/2)$, where $\boldsymbol{k_i}$ and $\boldsymbol{k_f}$ are the incoming and outgoing neutron wave vector, respectively, λ is the neutron wavelength, and θ the scattering angle, and the energy transfer which equals $\hbar\omega$, where $\hbar = h/2\pi$ and h is Planck's constant. Therefore, $S(\boldsymbol{Q}, \omega)$ uniquely contain information relating to both the timescale of motion and also the length scale over which motions occur [10]. For the protons in these HPW silica systems, the incoherent scattering measured in a quasielastic neutron scattering measurement is dominated by that from the protons, allowing the protons to be measured alone.

The present work aims to study proton diffusion in phosphotungstic acid-impregnated mesoporous silica and understand the effects of HPW content and SiO_2 support symmetry on the diffusion. *P6mm* symmetry silica is studied at two HPW loadings, as chosen in line with previous work [4–6] demonstrating the effectiveness of this PEM in fuel cell tests [4–6], with a disordered silica sample chosen for comparison, also studied at two HPW loadings.

2. Methods

2.1. Sample preparation

Two mesoporous silica samples, one disordered and the other with *P6mm* space-group symmetry, were prepared for this study, as informed by previous single cell tests using HPW-MSN PEMs [4–6]. Disordered mesoporous silica was purchased from Glantreo Ltd., Ireland, and *P6mm*-symmetry mesoporous silica was purchased from Unicarbon Shanghai Environmental Science and Technology Company Limited, China. To impregnate the silica with HPW, a water vacuum impregnation method was used as per previous methods [7]. HPW solution at 2.5 and 5.0 wt.% was prepared by dissolving HPW powder (Sigma–Aldrich, phosphotungstic acid hydrate, reagent grade) in deionized water. The dry silica was placed in a Büchner flask with a filter paper between the vacuum pump and the silica, and a rubber stopper sealed the top with a closed burette fitted to the assembly and the HPW solution added under vacuum. The vacuum pump was run for 6 h, after which the desired quantity of well shaken solution was added to the burette. The vacuum pump was turned off, and the solution added, before the vacuum pump was run for a further 10 min to remove any air and then was left to rest for 24 h. The material was filtered and washed with deionized water, and finally dried at 50–60 °C on a hotplate for ~4 h.

2.2. Sample composition and structure characterization

The proton conduction pathway in HPW-MSNs involves both intramolecular and intermolecular proton transfer, with

the overall barrier for proton diffusion determined by the intramolecular transfer [9]. The intramolecular proton transfer is closely related to the water content, which is shown to be affected by the size and symmetry of the mesopores [6]. Subsequently, the maximum pore size and porosity are related to the permeability of the membrane, but not directly to proton conductivity. Therefore, nitrogen adsorption/desorption and small and X-ray scattering measurements are commonly-used to characterize HPW-MSN pore size and structure. Elemental characterization allows the determination of HPW content.

2.2.1. Nitrogen adsorption/desorption measurement

Nitrogen gas adsorption/desorption isotherms for the silica prior to HPW impregnation were performed using a TriStar II 3020 V1.03 with a built in SiO_2 reference material. 0.25 cm^3 of sample was cooled to ~77 K and measurements taken over 8–10 h. The specific surface area was calculated using the Brunauer–Emmett–Teller (BET) method [17,18] and the pore size, volume, and distribution calculated using the Dollimore–Heal approach for *P6mm*-symmetry silica as it assumes cylindrical pores and the Barret, Joyner & Halenda method for the disordered silica which assumes spherical pores [19,20].

2.2.2. Small angle X-ray scattering

Laboratory-based small angle X-ray scattering was performed at the Western Australian Small Angle X-ray Scattering Faculty using a Bruker AXS Nanostar with a 2-dimensional Xe wire detector (1024 × 1024 pixels) at 1.541 Å over the $\boldsymbol{Q}$-range 0.014 to 0.85 $Å^{-1}$. Samples were mounted in a vacuum chamber and positioned 654 mm from the detector. Due to the vacuum environment, samples were pressed into a disk using potassium bromide (KBr) binder due to the very low signal. Background, instrumental noise, and KBr contributions were characterized using empty cell and KBr-only spectra.

2.2.3. Elemental characterisation

Inductively-coupled plasma optical emission spectroscopy (ICP-OES) was conducted on a Perkin Elmer Optima 7300DV. Samples were digested using a Milestone Ethos-1 microwave digester with hydrofluoric acid and analysed for W, Si, and P. The HPW concentration was calculated as the percentage by weight of the total sample, based on the Keggin unit containing 12 W atoms.

2.3. Sample function characterization

2.3.1. Electrochemical impedance spectroscopy

Electrochemical impedance spectroscopy measurements were performed using a Solartron SI 1260 Impedance/Gain Phase Analyser with ZPlot and data processed with equivalent circuits using ZVeiw software. Samples were pressed with a 13 mm diameter steel die at 2 tonnes for 2 min using polyethylene as a binder. Sample weight per volume varied significantly with increased HPW content necessitating geometric corrections specific to each sample due to differences in pellet density and dimensions. Due to high resistance of the samples and instrument limitations, measurements were taken at ~24 °C under a pure hydrogen atmosphere. Pure silica and HPW measurements were outside of the measurement capacity of the instrument, less than 10^{-12} S cm^{-1} for the silica and greater than 10^{-2} S cm^{-1} for the HPW. The equivalent circuit consisted of an initial resistance of 1 Ω to represent the fixed resistance of the instrument, and two consecutive resistor and parallel capacitor sets which represents the resistance and capacitance of the material bulk and the intergranular regions, respectively.

2.3.2. Quasielastic neutron scattering

Quasielastic neutron scattering was performed on PELICAN, the cold-neutron time-of-flight spectrometer [21] at the Australian Centre for Neutron Scattering at the Open-Pool Reactor Facility at the Australian Nuclear Science and Technology Organisation. For the samples analysed by QENS, the final deionized water was removed by vacuum and not a heat drying step. Approximately 1 g of sample was loaded into a flat-plate aluminium can of 0.5 mm thickness and oriented 45° to the incident beam. A bottom-loading cryostat was used to maintain the sample temperature at 300 K and $S(\boldsymbol{Q}, \omega)$ were collected for *P6mm* and amorphous mesoporous silica impregnated with the two loadings of HPW using 4.36 Å neutrons with higher harmonics removed using a cooled Be filter, affording a resolution at the elastic line of 207 μeV. A background spectrum for an empty can and instrument resolution function from a standard vanadium sample were also collected. Data corrections and manipulations were carried out using the LAMP software [22,23], with $S(\boldsymbol{Q}, \omega)$ binned in increments of $\Delta\boldsymbol{Q} = 0.1$ $Å^{-1}$ and $\Delta\omega = 0.02$ meV. $S(\boldsymbol{Q}, \omega)$ were analysed using empirical peak-fitting within the STRfit tool in LAMP. The $\boldsymbol{Q}$-dependence of extracted parameters was analysed using the software Origin.

3. Results and discussion

Nitrogen isotherm data (Fig. 1) reveals the pore size distribution of the silica prior to HPW impregnation. *P6mm*-

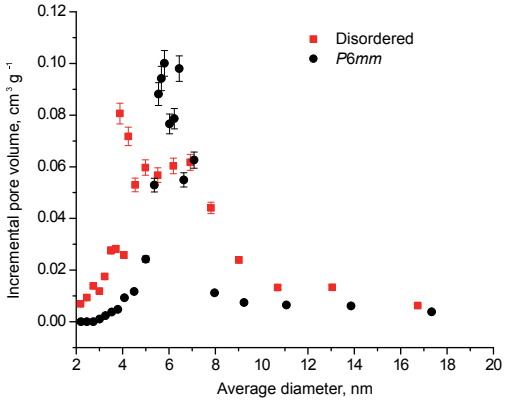

Fig. 1. Pore size distribution of mesoporous silica samples determined using nitrogen adsorption/desorption isotherm measurements. *P6mm*-symmetry silica is shown in black circles and disordered silica in red squares.

symmetry silica had a total pore volume of 0.831(23) $cm^3\ g^{-1}$ with an average pore size of 6.46(36) nm within the narrow 5–8 nm range. The disordered silica had a total pore volume of 0.676(19) $cm^3\ g^{-1}$ and an average pore size of 4.77(1) nm within the larger 3–12 nm range. The surface area was calculated to be 563(19) and 516(43) $m^2\ g^{-1}$ for the disordered and *P6mm* samples, respectively.

The concentration of HPW measured using ICP-OES is summarised in Table 1, which revealed an overall low concentration of HPW in all samples with HPW at two concentrations in each silica type. A higher level of HPW is found in the *P6mm*-symmetry silica relative to the disordered silica, likely as a result of its larger, ordered internal pore space.

Small angle X-ray scattering (SAXS) data for the HPW-impregnated silica with *P6mm* symmetry shows three peaks that can be indexed to the 11, 20, and 21 Miller indices, while the disordered porous silica SAXS data shows no peaks (Fig. 2). No features attributable to the HPW with $Pn\bar{3}\ m$ space group symmetry could be seen in either silica. These results further support the samples being *P6mm* and disordered silica with a low concentration of HPW.

Electrochemical impedance spectroscopy measurements (Table 2) reveal a marginal increase in conductivity with increased HPW concentration, as well as a more significant order of magnitude increase in conductivity of *P6mm* over disordered silica. Commensurate with this, the QENS data, $S(\boldsymbol{Q}, \omega)$ indicates significantly greater signal broadening for the *P6mm* than the disordered silica samples (Fig. 3), indicating faster proton diffusion. Qualitatively, there appears "pinching" in the $\boldsymbol{Q}$-dependent broadening of $S(\boldsymbol{Q}, \omega)$ which is more evident for the disordered than the *P6mm* silica and marked by the dashed lines and arrows in Fig. 3, occurring at $\mathbf{Q}$ ~1.8 $Å^{-1}$. This saddle point indicates a change in motion at this lengthscale.

The $S(\boldsymbol{Q}, \omega)$ for all four samples could be described using the phenomenological model [16]:

$$S(\boldsymbol{Q},\omega) = \left\{ A\left[\frac{\Gamma_1}{\pi\left(\Gamma_1^2+\omega^2\right)}\right] + B\left[\frac{\Gamma_2}{\pi\left(\Gamma_2^2+\omega^2\right)}\right] \right\} \otimes R(\boldsymbol{Q},\omega) + C \tag{1}$$

where two Lorentzian functions were required, each with half width at half maximum (HWHM) of Γ_1 and Γ_2 that varied as a function of $\boldsymbol{Q}$ with number densities of associated scattering of A and B, respectively. $R(\boldsymbol{Q}, \omega)$ is the resolution function and C is a linear background. Data were fitted in the range −3 to 3 meV from $\boldsymbol{Q} = 0.5$ to 2.2 $Å^{-1}$. A typical fit of this model to data is shown in Fig. 4 and all fit results are included in the Supporting Information.

Table 1
HPW concentration in samples determined using inductively-coupled plasma optical emission spectroscopy.

HPW concentration solution, wt.%	HPW concentration *P6mm* silica, wt.%	HPW concentration disordered silica, wt.%
2.5	0.15 (1)	0.10 (1)
5.0	0.30 (2)	0.14 (1)

For clarity we will refer to the first Lorentzian as component one, and the second as component two. Each Lorentzian function represents a different population of protons moving on different timescales, and the pre-factors in Eq. (2), A and B, indicated that these populations are approximately equal in size. Clear trends in $\boldsymbol{Q}$-dependent broadening that are indicative of the geometry of motion are observed for both populations.

Component 1 shows $\boldsymbol{Q}$-dependent broadening that is characteristic of the translational diffusion of protons occurring via a jump-diffusion mechanism [16,24] and is similar between both silica support types and HPW loading (Fig. 5). Importantly, component 1 is almost twice as broad in the *P6mm* silica than in the disordered data, clearly evidencing faster diffusion. The saddle point in the $S(\boldsymbol{Q}, \omega)$ in Fig. 3 is captured by this model, and notably occurs for all four samples at approximately the same $\boldsymbol{Q}$, suggesting that the geometry of proton motion is similar for all samples. The $\boldsymbol{Q}$-dependence of component 1 broadening could be described by the Chudley–Elliot jump-diffusion model [25], which describes a population of protons with a residence time (τ) at a site before moving instantaneously to another site with a jump length, d is the translational self-diffusion constant of the protons, D relates to d and τ [16]:

$$\Delta\Gamma_1(\boldsymbol{Q}) = \frac{1}{\tau}\left(1 - \frac{\sin(\boldsymbol{Q}d)}{\boldsymbol{Q}d}\right) \tag{2}$$

$$D = d^2/(6\tau) \tag{3}$$

It is not uncommon for diffusing protons in solids, particularly oxides, to undergo complex diffusion processes, necessitating more sophisticated models to explain the $\boldsymbol{Q}$-dependence of component broadening [26]. Whilst further information may be gained by molecular dynamics simulations, the very large number of atoms required to represent such systems and the absence of structural detail for the disordered system severely limits a detailed analysis. This is not an uncommon problem, and the fit of the Chudley–Elliot diffusion model to component 1 broadening is within the range of those fairly typical for quasielastic neutron scattering data [16,24], and the standard errors reported for the derived parameters (Table 3) are reasonable. It is the overall shape of the $\boldsymbol{Q}$-dependent broadening that defines key parameters for the process, these being the rate of broadening in the lower $\boldsymbol{Q}$ region and the $\boldsymbol{Q}$ of the maximum Γ_1 where the broadening tapers. Importantly, while not accurately representing the exact process, the Chudley–Elliot diffusion model captures these main features reasonably well, yielding a higher D for the *P6mm* relative to the disordered silica and an identical jump length within 1 estimated standard deviation for all samples, as indicated clearly by the data.

The residence time of component 1 protons is significantly different between the silica support types, with that of protons in the disordered silica being approximately double that for

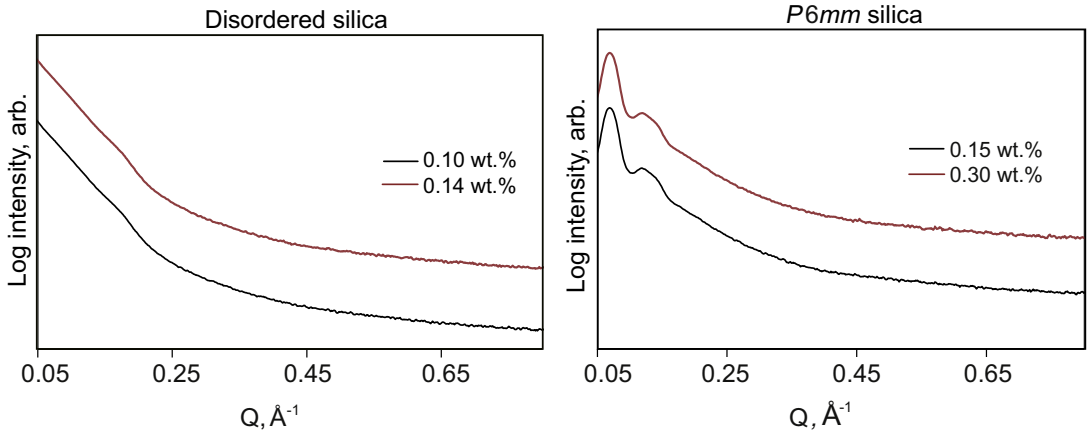

Fig. 2. SAXS data for disordered and *P6mm*-symmetry mesoporous silica impregnated with various concentrations of HPW (concentrations determined from ICP-OES).

Table 2
Results of electrochemical impedance spectroscopy measurements.

Sample	Conductivity, S cm^{-1}
Disordered 0.10 wt.%	1.7×10^{-6}
Disordered 0.14 wt.%	3.9×10^{-6}
P6mm 0.15 wt.%	2.1×10^{-5}
P6mm 0.30 wt.%	2.9×10^{-5}

protons in the ordered *P6mm* matrix. A much smaller difference was observed when the HPW loading was varied, and in both silica types the residence time decreased with increased HPW content. Given the identical jump lengths for component 1 protons in all four samples, the higher D of these protons in the *P6mm* silica clearly arises from a reduced site residence time. Previous studies on HPW on silica have noted higher conductivity in more acidic conditions [2], and significant differences in surface acidity of *P6mm* symmetry and disordered silica have been found [27,28]. Notably, the surface of *P6mm* symmetry silica is highly acidic as a result of strained Si−O bonding in the structure, while disordered silica is found to be closer in acidity to bulk SiO_2 where surface protonation is more dependent on the pH the material is exposed to. The lower residence time of component 1 protons at sites within the *P6mm* silica may arise from more acidic conditions compared to those within the disordered silica, reducing the energy barrier for proton transfer. The reduced residence time results in faster diffusion and is consistent with the conductivity measurements that show higher conductivity of HPW-impregnated *P6mm* than disordered silica, and also at higher HPW loadings.

The width of component 2 in the $S(\boldsymbol{Q}, \omega)$ model in all four silica samples is an order of magnitude greater than component 1, indicating a faster diffusive process. Importantly, the width of component 2 does not change considerably with either silica type or HPW concentration, indicating that proton conductivity is limited by the slower diffusive process of component 1 protons (Fig. 6). For all samples, component 2 broadens initially with $\boldsymbol{Q}$ and then tapers at $\mathbf{Q}$ ~1.1 Å^{-1} before broadening less quickly at higher $\boldsymbol{Q}$. There is a further feature at $\mathbf{Q}$ ~1.4 Å^{-1} in both samples where there is a narrowing of the component before further broadening at higher $\boldsymbol{Q}$. The overall similarity of the features suggests, as with component 1 protons, a similar motion of component 2 protons in all four samples. The greater prominence of the feature at $\mathbf{Q}$ ~1.4 Å^{-1} in the ordered *P6mm* samples suggests a mechanism of proton

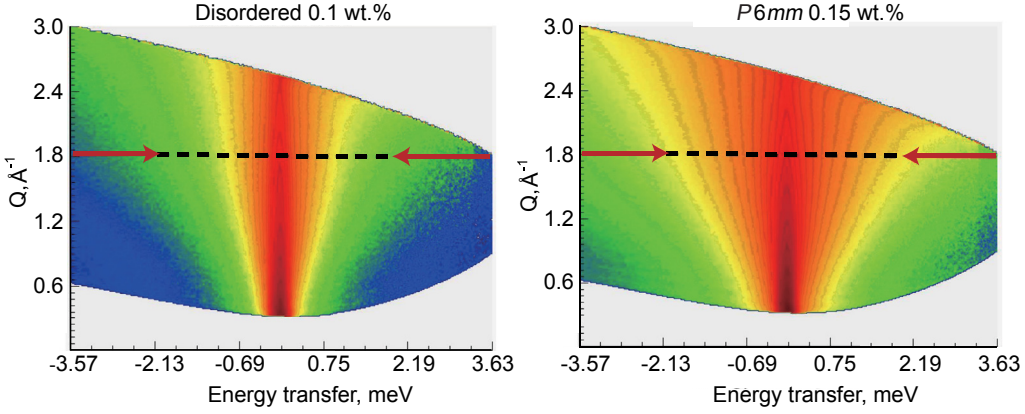

Fig. 3. $S(\boldsymbol{Q}, \omega)$ shown as a contour plot with intensity in colour (intensity is shown red, yellow, green, and blue from highest to lowest, respectively) for disordered and *P6mm*-symmetry mesoporous silica impregnated with the lowest concentration of HPW (concentrations determined from ICP-OES).

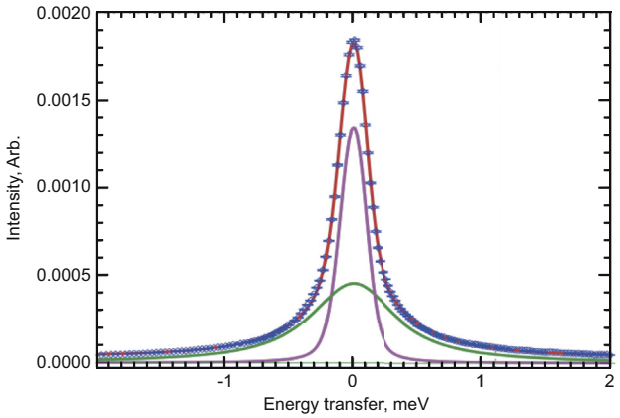

Fig. 4. QENS spectrum for the disordered silica with 0.10 wt.% HPW at $\mathbf{Q} = 1.6(15)$ Å^{-1} (blue points with error bars shown). The fit of a model to the data (red line) containing two Lorentzian components (green and pink lines) along with a flat background (green line) is also shown.

diffusion that is spatially anisotropic, which is averaged in the disordered silica matrix samples, supressing the feature.

The $\boldsymbol{Q}$-dependence of component 2 broadening does not fit any of the well-known jump-diffusion models typical for protons in solids [16,24], with existing models capturing either the $\boldsymbol{Q}$-dependent broadening at lower $\boldsymbol{Q}$ or the feature at $\mathbf{Q}$ ~1.4 Å^{-1} and beyond, but not both. This suggests a mechanism that is more complex than a simple single population. Again, the diffusion process is complicated and cannot be explained without more sophisticated diffusion models necessitating further information concerning the material structure and relative position of proton interaction sites [26]. Nevertheless, to understand the differences in the $\boldsymbol{Q}$-dependent broadening, we approximate the average processes to the Singwi and Sjölander jump-type diffusion mechanism [29] in which a population of protons undergo translational diffusion alternating between oscillatory and jump processes. In this model the jump process has a residence time (τ) at a site and a distribution of jump lengths where the mean-square jump length is $<r^2>$, and the proton diffusion constant, D, is related to d ($=\sqrt{<r^2>}$) and τ as per Eq. (3):

Table 3
Fit results of the Chudley–Elliot diffusion model to component 1 of the $S(\boldsymbol{Q}, \omega)$. τ is residence time in picoseconds, d is the jump distance in Å, and D is the diffusion coefficient in cm^2 s^{-1}.

Sample	Component 1		
	τ, ps	d, Å	D, cm^2 s^{-1}
Disordered 0.10 wt.%	26.2 (9)	3.1 (1)	6.0 (5) × 10^{-6}
Disordered 0.14 wt.%	24.9 (8)	3.0 (1)	6.2 (5) × 10^{-6}
P6mm 0.15 wt.%	12.3 (3)	3.0 (9)	1.20 (7) × 10^{-5}
P6mm 0.30 wt.%	11.7 (3)	3.01 (9)	1.29 (8) × 10^{-5}

$$\Delta\Gamma_1(\boldsymbol{Q}) = \frac{1}{6\tau}\left(\frac{\boldsymbol{Q}^2 <r^2>}{1 + \boldsymbol{Q}^2 <r^2>/6}\right) \quad (4)$$

The relatively-poor fit of the Singwi and Sjölander model to component 2 broadening results in a large estimated standard deviation for the determined root mean average jump length and therefore, no significant difference between these was found for the four samples (Table 4). The residence time for protons at sites is, however, different between silica types, being slightly lower in *P6mm* structured relative to the disordered silica. While not capturing the true diffusion mechanism, the approximation to the Singwi and Sjölander type jump-diffusion reveals differences between the *P6mm* and disordered silica samples that reflect those of the slower-moving population of diffusing protons (component 1), evidencing further a lower activation energy for jump-diffusion in the *P6mm* silica.

4. Conclusion

Proton diffusion was studied using quasielastic neutron scattering in phosphotungstic acid impregnated mesoporous silica and correlated to proton conduction, as measured using electrical impedance spectroscopy. Two types of mesoporous silica were studied, one with an ordered *P6mm* symmetry structure and another disordered structure, each at a lower and

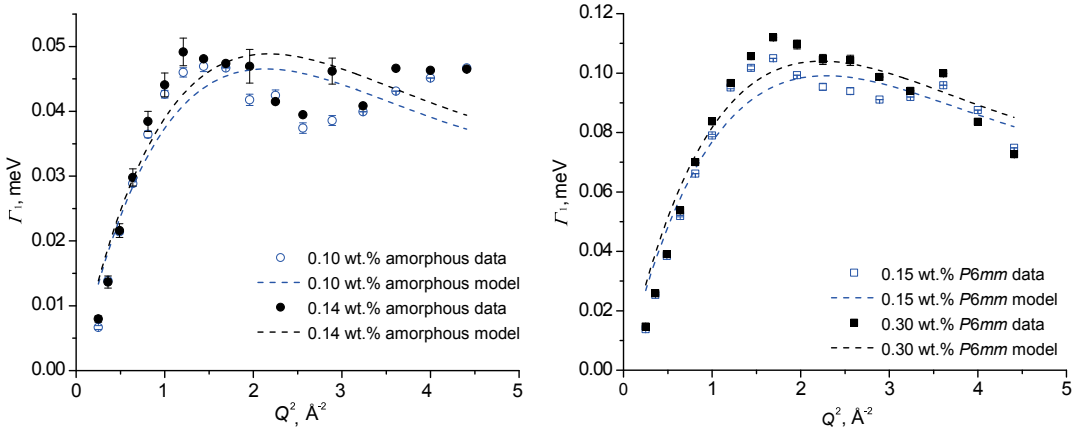

Fig. 5. $\boldsymbol{Q}^2$ dependence of the width of the first component in the $S(\boldsymbol{Q}, \omega)$ model for disordered and *P6mm*-space group mesoporous silica impregnated with various concentrations of HPW.

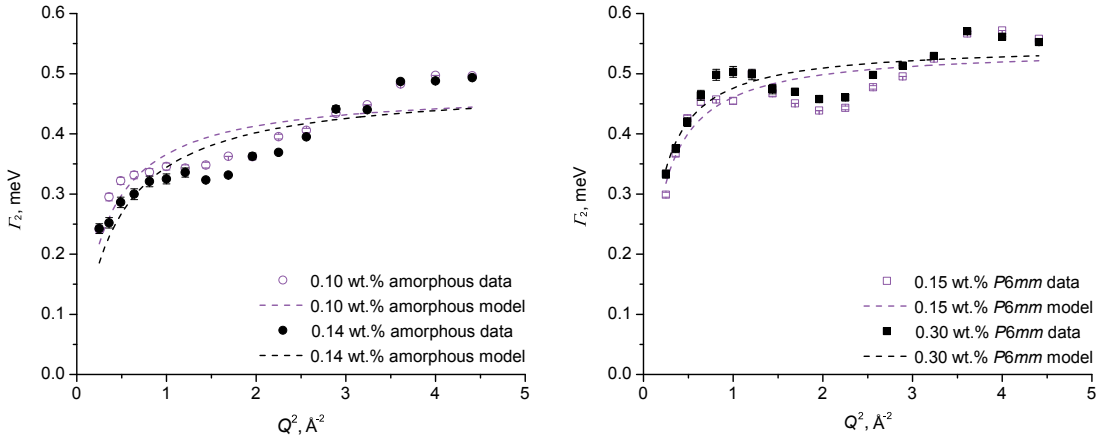

Fig. 6. Q^2 dependence of the width of the second component of the $S(Q, \omega)$ model for disordered and *P6mm*-space group mesoporous silica impregnated with various concentrations of HPW.

Table 4
Fit results of the Singwi and Sjölander diffusion model to component 2 of the $S(Q, \omega)$. τ is residence time in picoseconds, d is the jump distance in Å, and D is the diffusion coefficient in $cm^2\ s^{-1}$.

Sample	Component 2		
	τ, ps	d Å	D, $cm^2\ s^{-1}$
Disordered 0.10 wt.%	2.11 (9)	4.5 (5)	$1.6\ (3) \times 10^{-4}$
Disordered 0.14 wt.%	2.1 (1)	3.9 (4)	$1.2\ (2) \times 10^{-4}$
P6mm 0.15 wt.%	1.84 (6)	5.8 (6)	$3.1\ (6) \times 10^{-4}$
P6mm 0.30 wt.%	1.82 (4)	6.3 (6)	$3.6\ (6) \times 10^{-4}$

higher concentrations of phosphotungstic acid. Overall, the structure of the mesoporous silica support had a major effect on the proton conduction, while very little difference was made by changes in phosphotungstic acid concentration at the tested level. Quasielastic neutron scattering revealed two populations of diffusing protons, of approximately similar size, in all four samples. Proton diffusion was found to be controlled almost entirely by the slower-moving proton population, via a jump-diffusion mechanism in which the jump length remained constant and the residence time of protons changed considerably with the type of silica support used, with lower residence times resulting in faster proton diffusion. The higher conductivity of phosphotungstic acid impregnated mesoporous silica proton conducting membranes containing *P6mm* symmetry over disordered silica likely arises as a result of the relatively-more acidic conditions, reducing the energy barrier for proton transfer.

Conflict of interest

The authors declare that there is no conflict of interest regarding the publication of this paper.

Acknowledgements

Roland De Marco, Krystina Lamb, San Ping Jiang, and John Bartlett acknowledge support from Australian Research Council Discovery Project DP120102325, the Centre for Microscopy and Microanalysis at the University of Queensland, and Curtin University. Krystina Lamb is grateful to the Australian Institute for Nuclear Science and Engineering for support through a Post-Graduate Research Award, and to the School of Agriculture and Food Science technical services of the University of Queensland for inductively-coupled plasma optical emission spectroscopy measurements.

Appendix A. Supplementary data

Supplementary data related to this article can be found at http://dx.doi.org/10.1016/j.gee.2017.06.007.

References

[1] W.H.J. Hogarth, J.C. Diniz da Costa, G.Q. (Max) Lu, J. Power Sources 142 (2005) 223–237.
[2] N. Azuma, R. Ohtsuka, Y. Morioka, H. Kosugi, J. Kobayashi, J. Mater. Chem. 1 (1991) 989–996.
[3] H.L. Tang, M. Pan, S.F. Lu, J.L. Lu, S.P. Jiang, Chem. Commun. 46 (2010) 4351–4353.
[4] S.F. Lu, D.L. Wang, S.P. Jiang, Y. Xiang, J.L. Lu, J. Zeng, Adv. Mater. 22 (2010) 971–976.
[5] J. Zeng, Y.H. Zhou, L. Li, S.P. Jiang, Phys. Chem. Chem. Phys. 13 (2011) 10249–10257.
[6] J. Zeng, P.K. Shen, S.F. Lu, Y. Xiang, L. Li, R. De Marco, S.P. Jiang, J. Membr. Sci. 397 (2012) 92–101.
[7] J. Zeng, S.P. Jiang, J. Phys. Chem. C 115 (2011) 11854–11863.
[8] H.L. Tang, M. Pan, S.P. Jiang, Dalton Trans. 40 (2011) 5220–5227.
[9] Y. Zhou, J. Yang, H. Su, J. Zeng, S.P. Jiang, W.A. Goddard, J. Am. Chem. Soc. 136 (2014) 4954–4964.
[10] G.M. Brown, M.R. Noe-Spirlet, W.R. Busing, H.A. Levy, Acta Crystallogr. B33 (1977) 1038–1046.
[11] J. Janik, R. Davis, M. Neurock, J. Amer. Chem. Soc. 127 (2005) 5238–5245.
[12] J. Yang, M. Janic, D. Ma, A. Zheng, M. Zhang, M. Neurock, et al., J. Amer. Chem. Soc. 127 (2005) 18274–18280.
[13] H. Li, M. Nogami, Adv. Mater. 12 (2002) 912–914.
[14] M. Bhure, I. Kumar, A. Natu, R. Chikate, C. Rode, Catal. Commun. 9 (2008) 1863–1868.
[15] V.M. Mastikhin, S.M. Kulikov, A.V. Nosov, I.V. Kozhevnikov, I.L. Mudrakovsky, M.N. Timofeeva, J. Mol. Catal. 60 (1990) 65–70.

[16] M. Bée, Quasielastic Neutron Scattering Principles and Applications in Solid State Chemistry, Biology, and Materials Science, first ed., IOP Publishing Ltd, Bristol, England, 1988.
[17] S. Brunauer, P.H. Emmett, E. Teller, J. Am. Chem. Soc. 60 (1938) 309−319.
[18] M. Jaroniec, M. Kruk, Langmuir 15 (1999) 5410−5413.
[19] P. Ravikovitch, A. Neimark, J. Phys. Chem. B 105 (2001) 6817−6823.
[20] E. Barrett, L. Joyner, P. Halenda, Ind. Eng. Chem. Res. 44 (1952) 1827−1833.
[21] D. Yu, R.A. Mole, T. Noakes, S. Kennedy, R. Robinson, J. Phys. Soc. Jpn. 82 (2013). SA027.
[22] LAMP. http://www.ill.eu/instruments-support/computing-for-science/cs-software/all-software/lamp.
[23] D. Richards, M. Ferrands, G.J. Kearly, J. Neutron Res. 4 (1996) 33−39.
[24] H. Jobic, D. Theodorou, Microporous Mesoporous Mater. 102 (2007) 21−50.
[25] C.T. Chudley, R.J. Elliott, Proc. Phys. Soc. Lond. 77 (1961) 353−361.
[26] M. Karlsson, Phys. Chem. Chem. Phys. 17 (2015) 26−38.
[27] T. Yamamoto, S. Mori, T. Kawaguchi, T. Tanaka, K. Nakanishi, T. Ohta, J. Kawai, J. Phys. Chem. C 112 (2008) 328−331.
[28] A. Pettersson, J. Rosenholm, Langmuir 22 (2008) 8447−8454.
[29] K.S. Singwi, A. Sjölander, Phys. Rev. 120 (1960) 1093−1102.